Macromolecules
COMMUNICATION TO THE EDITOR

Macromolecules **2010**, *43*, 3169–3172 **3169**
DOI: 10.1021/ma9028695

True Surface Topography and Nanomechanical Mapping Measurements on Block Copolymers with Atomic Force Microscopy

Dong Wang,* So Fujinami, Ken Nakajima, and Toshio Nishi

WPI Advanced Institute for Materials Research, Tohoku University, 2-1-1 Katahira, Aoba, Sendai 980-8577, Japan

Received January 2, 2010
Revised Manuscript Received March 1, 2010

1. Introduction. Block copolymers (BCPs) have attracted increased interest in recent years. The highly ordered nanostructures formed by self-assembly can be found in a wide range of promising applications.[1−6] To date, most of the studies on BCP nanostructures have been done using small-angle X-ray scattering (SAXS) and electron microscopy with proper staining techniques.[7] However, each of these techniques has limitations. The radiation and staining of electron microscopy may damage and change the delicate structure of these BCPs, while neither SAXS nor electron microscopy techniques can be used to determine mechanical information on such materials. In order to understand and develop advanced BCP materials, there is great importance to investigate these samples for identifying phase separated topography, composition, and mechanical properties of individual blocks.

Recently developed atomic force microscopy (AFM) nanomechanical mapping techniques such as the AFM tapping mode using torsional harmonic cantilevers,[8,9] the band excitation method,[10] the contact resonance based technique,[11] and the force volume mode (FV)[12,13] have become simple and efficient methods to obtain the elastic and adhesive properties of materials with surface heterogeneity. In this work, we report a quantitative method to obtain nanomechanical mapping data of poly(styrene-*b*-ethylene-*co*-butylene-*b*-styrene) (SEBS) triblock copolymers. Our method is different from other current techniques and emphasizes the AFM force volume imaging technique together with Johnson−Kendall−Robert[14] (JKR) analysis. With our technique, high-resolution maps of Young's modulus, adhesive energy, and topography can be obtained simultaneously in a single scan. In addition, we introduce a procedure to rebuild a true height image by which the real surface topography of samples can be determined.

2. Experimental Section. A SEBS sample was supplied by Asahi KASEI Corp. without further treatment. The number-average molecular weight, M_n, and the weight fraction of polystryrene (PS) are 50 000 and 0.30, respectively. The film samples with thickness about 10 μm were prepared by solvent-casting a 0.04 g/mL SEBS toluene solution onto cleaned glass slides. The as-prepared films were first dried in a fume hood for 1 day and then in vacuum at room temperature for another 3 days to remove residual solvent.

Nanomechanical measurements were operated in force volume (FV) mode on a commercial AFM system (MultiMode with a NanoScope V controller) under ambient conditions. The samples were scanned at constant force using an *E* scanner and triangular Si_3N_4 cantilevers with nominal spring constant of 0.32 N/m (SNL-10, Veecoprobes). An actual spring constant of 0.397 ± 0.005 N/m was measured by the thermal tune method. Force curves were collected over randomly selected surface areas of 1 μm × 1 μm at a resolution of 128 × 128 pixels. In order to eliminate the effect of substrate stiffness, the value of the trigger set point (3 nm) was far less than the 1% of the film thickness. The obtained force curves were analyzed using JKR contact mechanics. According to this model, the Young's modulus *E* and adhesive energy *w* are expressed by the following two equations:[15]

$$E = \frac{3(1-\nu^2)}{4}\frac{1.27F_1}{\sqrt{R(\delta_0-\delta_1)^3}} \quad (1)$$

$$w = -\frac{2F_1}{3\pi R} \quad (2)$$

where ν is the Poission's ratio, *R* is the radius of curvature for the probe tip, δ is the sample deformation, and F_1 is the maximum adhesive force as shown in Figure 2S. The Supporting Information shows the detailed analysis procedures.

For comparison, tapping mode data were also obtained using the same AFM and a silicon cantilever with a nominal spring constant of 20−80 N/m (MPP-11100-10, Veecoprobes). The moderate tapping force corresponding to set-point ratios of ~0.70 was used.

3. Results and Discussion. The triblock copolymer SEBS consisting of hard and soft components that usually exhibits a lamellar phase-separated morphology has been widely studied by AFM techniques.[16−19] Figure 1 shows the tapping mode topographic (height) image of SEBS film along with the corresponding sectional analysis. As expected, the well-ordered lamellar morphology consisting of bright and dark nanophasic domains is observed. The lamellar morphology gives a domain width of 12−15 nm for the bright regions and 13−18 nm for dark regions. The specific value of periodicity distance determined by fast Fourier two-dimensional-power spectrum is 26.8 ± 2.5 nm. Using AFM tapping mode, the measured periodicity distances of SEBS samples (having the same composition as the sample's used in the present study) by Motomatsu et al.[16] and Bhowmick et al.[20] are 30.8 ± 1.1 and 23 ± 2 nm, respectively. The periodicity variation may relate to the material characteristics, such as molecular weight.[21−23] Other possibilities include sample preparation such as solvent or temperature effects. It is worthy of mention that the periodicity distance calculated by Helfand and Wasserman in bulk copolymers is 26−28 nm,[22,23] and this result has been confirmed its accuracy by comparing it with many experimental data obtained by TEM or SAXS.[16] Therefore, the measured value 26.8 ± 2.5 nm in this work is in well agreement. However, the topography data alone provide little information about the chemical and mechanical heterogeneity of the SEBS film. Without further analysis, identification of the bright or dark regions is not possible. In other reports, some researchers have assigned the bright regions to the hard PS component and dark regions to the soft rubbery ethylene-*co*-butylene (PEB) component.[16,20] In general, however, assigning chemical composition to the

*To whom correspondence should be addressed. E-mail: wangdthu@wpi-aimr.tohoku.ac.jp.

Published on Web 03/05/2010

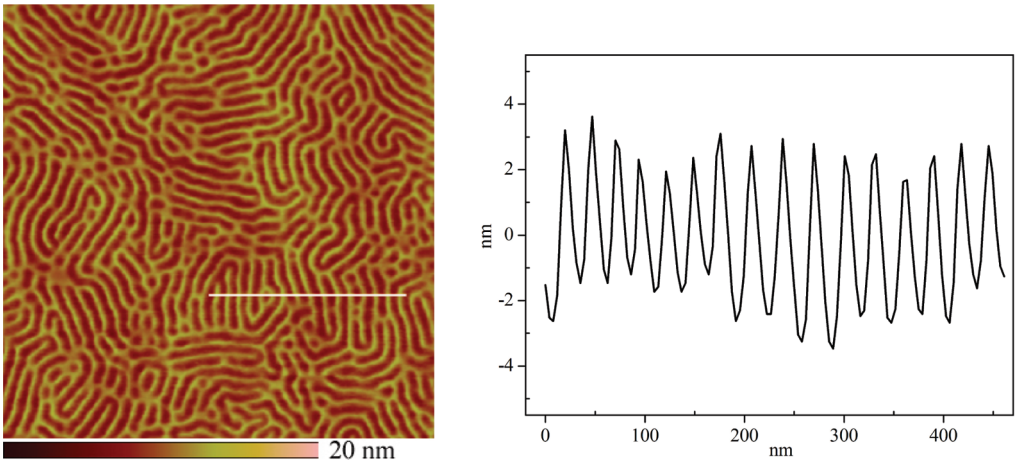

Figure 1. Tapping mode AFM: (a) height image obtained using light tapping and (b) sectional analysis of SEBS film. The scan size is 1 μm. Set-point ratio is 0.68.

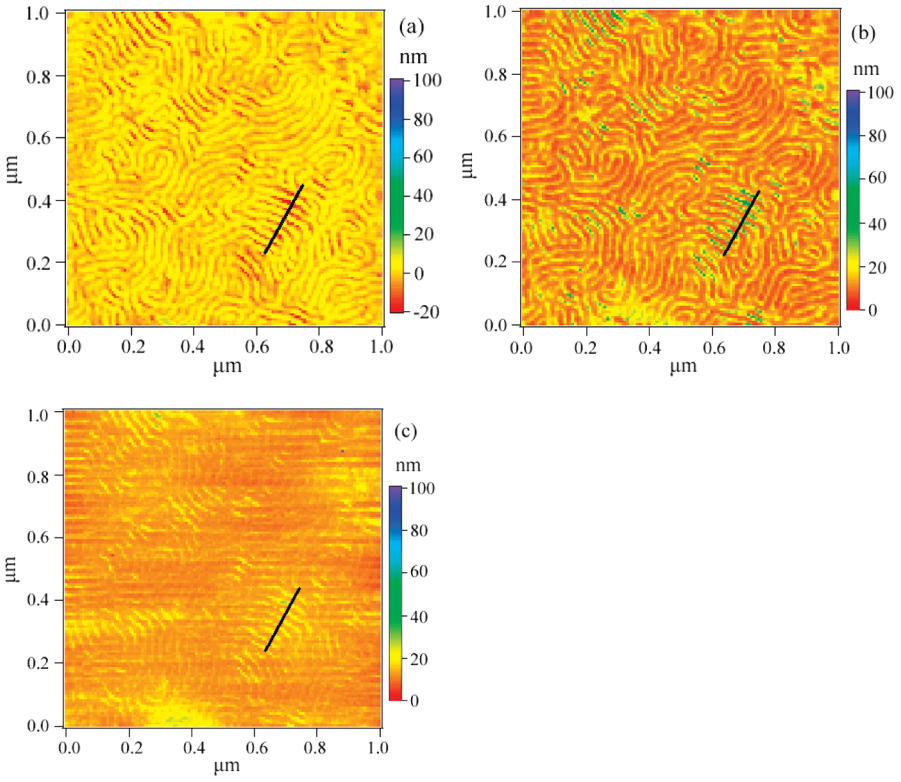

Figure 2. Nanomechanical mapping results: (a) original height image, (b) deformation image, and (c) true height image of SEBS film prepared by solvent-casting technique.

features observed in height and phase images is difficult.[24] Further, the assignment of the bright or dark contrast to the hard or soft domain in phase imaging is not always straightforward. For example, several studies have assigned the brighter regions to the softer material and the darker regions to the stiffer material.[25,26] In order to provide an easy and efficient method for identifying the composition and investigating the mechanical properties of different regions, nanomechanical mapping measurements were performed.

In tapping mode, the height images are affected by the sample deformation caused by the force between the probe tip and the sample.[25,26] Such images usually lead us to misinterpret them as topographies. This situation will become more serious when the sample is soft materials such as polymeric or biorelated materials. Here, we first demonstrate a procedure by which the true height images can be obtained in the nanomechanical mapping measurement. Figure 2 shows the generated original height, sample deformation, and true height images. Shown in Figure 2a is the original height image directly obtained from the force volume mode. It contains artifacts due to the low elastic modulus of rubbery PEB component. The sample deformation δ is calculated by subtracting the cantilever deflection Δ from the scanner displacement z ($\delta = z - \Delta$). Then, two-dimensional arrays of sample deformation values can be regarded as a sample deformation image (Figure 2b). The true height image can be considered as the superimposition of the original height image and the sample deformation

image. The weak contrast of the true height image is due to large compensation of the deformation at soft PEB regions. Even though, it reveals the real surface topography of the SEBS films prepared by solvent casting technique. By comparing the section analysis of the original height and true height images (Figure 3), it is found that the topography is totally reversed. The higher and lower regions in the original height image become lower and higher regions in the true height image. The height contrast reverses is due to the large deformation (Figure 3) caused by the force between the probe tip and the sample. On the other hand, the calculated tapping force in the tapping mode experiment is about 0.35−0.45 nN, which is almost equal to one-third of the trigger threshold of 1.2 nN in the FV mode. The corresponding deformation in the tapping mode is calculated to be almost half of the deformation in FV mode. It indicates that the deformation of PS and PEB blocks are about 5 and 15 nm, respectively. Considering that the apparent height difference in the tapping mode height image is ~4.5 nm, it can be concluded that the true topography should be the inverse of tapping mode height image. Then, similar to the original height image obtained from FV mode, the tapping mode height image is also an artifact due to the large deformation. However, the reconstructed true height image reveals the true surface topography and shows that the softer PEB blocks are actually higher than the stiffer PS blocks. This finding clearly demonstrates that both the tapping mode height image and the FV original height image of SEBS films are artifacts. Therefore, we may conclude that the reconstruction procedure is valid enough to claim that the obtained height image represents the true topographic feature free from sample deformation.

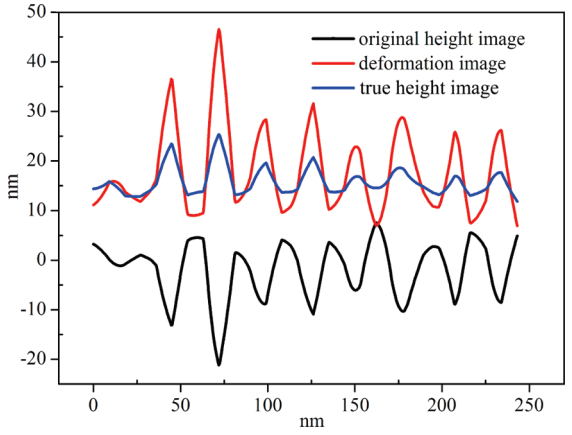

Figure 3. Section analysis of the original height, deformation, and true height image.

Figure 4 shows simultaneously generated maps of the Young's modulus and adhesive energy. Both the Young's modulus and adhesive energy distribution images show phase-separated lamellar morphology. The corresponding modulus and adhesive energy profile across a section reveals the two chemical blocks have a large difference in modulus and adhesive energy values. In the Young's modulus image, the light green areas with higher Young's modulus are considered to be the hard PS blocks, while the red areas with lower Young's modulus are considered to be the soft PEB blocks. Two typical force−deformation curves corresponding to the two points indicated by circles in the Young's modulus image (Figure 4a) are shown in Figure 5. The curve fitting against JKR contact is also superimposed in each case. The results show that JKR analysis of the withdrawing process is fitted well for elastic PS component. However, deviation appears for the viscoelastic PEB component (shown in Figure 5b) because of the viscoelastic effect. Figure 3S (Supporting Information) shows the map of deviated work, which clarifies the difference of viscoelasticity between PS and PEB. The Young's modulus is calculated as 53.3 ± 5.4 MPa for white circle and 10.6 ± 3.2 MPa for dark circle. We thus further demonstrate that the light green areas correspond to PS blocks and the red areas to PEB blocks. Using the same evaluation method, we also investigate the Young's modulus of bulk PS and PEB films. The measured modulus value of glassy PS and rubbery PEB is

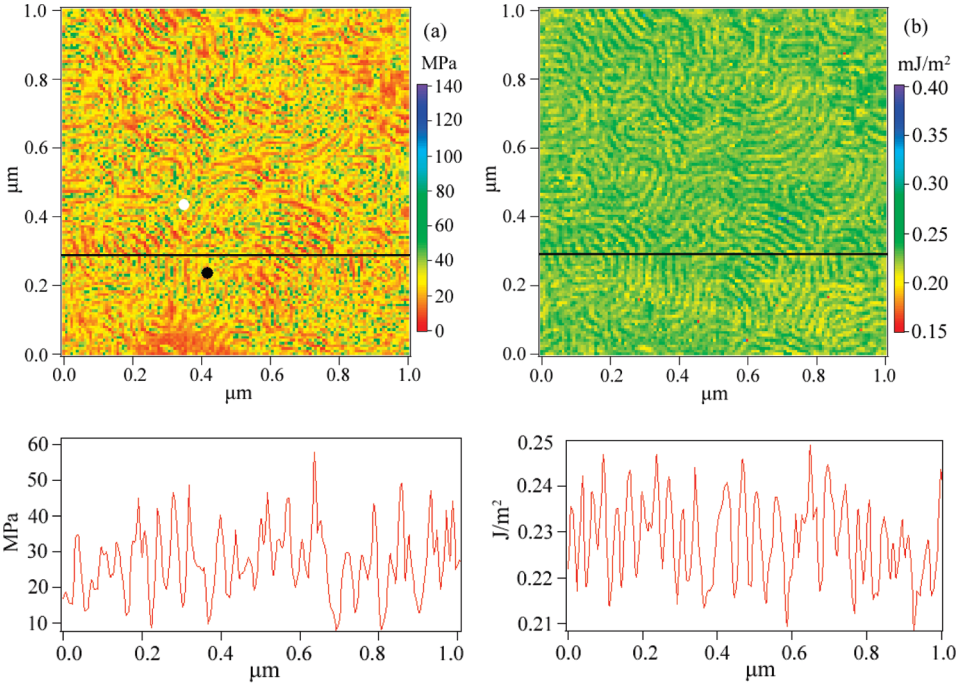

Figure 4. Nanomechanical mapping results: (a) Young's modulus distribution image and (b) adhesive energy distribution image of SEBS film. Numerical values in each image across the sections indicated by the line in (a) and (b) are given below the images.

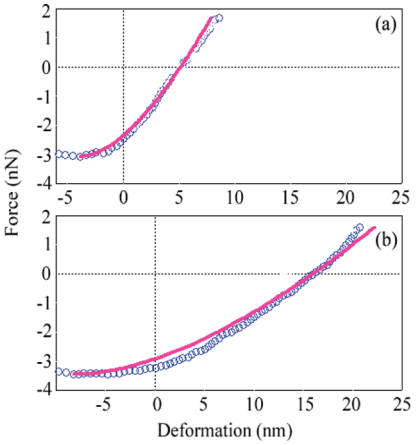

Figure 5. Force−deformation curves of local points indicated by the circles in Figure 4a. The curve-fitting against JKR contact was superimposed on each curve. (a) PS region (white circle), 53.3 ± 5.4 MPa. (b) PEB region (black circle), 10.6 ± 3.2 MPa.

2.23 ± 0.51 GPa and 13.64 ± 0.68 MPa, respectively. Therefore, the observed modulus on PEB block agrees with bulk value, while PS block's demonstrates a dramatic decrease in stiffness. This decrease may be due to the microstructure effect that the soft PEB blocks surround and support the PS blocks underneath.[16,29−31] Other possibilities are that there are some uncertain factors such as the contact area, tip geometry, and the local value of Poisson's ratio. The adhesive energy image also differentiates the two chemical blocks of the copolymer. However, the adhesive energy contrast between the hard PS and soft PEB blocks is inverted in comparison to the Young's modulus map. The stiffer PS blocks provide lower adhesive energy than the soft PEB blocks. The calculated adhesive energy of PS and PEB components corresponding to the two points indicated in the Young's modulus image is 0.210 ± 0.004 and 0.243 ± 0.006 J/m^2, respectively. Comparing with the measured adhesive energy of the bulk PS (0.457 ± 0.037 J/m^2) and PEB (1.942 ± 0.094 J/m^2), the big discrepancy may relate to the interaction between tip and sample surface. The determined adhesive energy in this work includes all interactions between the tip and sample surface, such as capillary force, which makes the measured adhesive energy is very high.

4. Conclusions. In summary, we have investigated the nanomechanical mapping of SEBS triblock copolymers by the AFM force volume mode in combination with an analysis procedure based on JKR contact mechanics. The true topography, elastic modulus, and adhesive energy together with the original height and deformation images have been obtained simultaneously in a single scan. The calculated local Young's modulus and adhesive energy are about 53.3 ± 5.4 MPa and 0.210 ± 0.004 J/m^2 for the hard PS blocks and 10.6 ± 3.2 MPa and 0.243 ± 0.006 J/m^2 for the soft PEB blocks. The Young's modulus value of the soft PEB component agrees well with the bulk viscoelastic properties, whereas the measured value of hard PS shows a dramatic decrease in stiffness because of the microstructure effect. The original topography directly obtained from the force volume mode and tapping mode is demonstrated to be an artifact, which is never realized by constant force feedback. These results will be helpful for identifying the composition and investigating the mechanical properties and topography of the chemically and mechanically heterogeneous materials at a nanoscale.

Acknowledgment. The authors thank Dr. Kazuya Nagata of the Asahi Kasei Chemicals Corp. for technical assistance.

Supporting Information Available: Analysis procedure and Figure 3S. This material is available free of charge via the Internet at http://pubs.acs.org.

References and Notes

(1) Park, C.; Yoon, J.; Thomas, E. L. *Polymer* **2003**, *44*, 6725–6760.
(2) Ludwigs, S.; Böker, A.; Voronov, A.; Rehse, N.; Magerle, R.; Krausch, G. *Nat. Mater.* **2003**, *2*, 744–747.
(3) Bates, F. S.; Fredrickson, G. H. *Phys. Today* **1999**, *52*, 32–38.
(4) Park, S.; Lee, D. H.; Xu, J.; Kim, B.; Hong, S. W.; Jeong, U.; Xu, T.; Russell, T. P. *Science* **2009**, *323*, 1030–1033.
(5) Bang, J.; Kim, S. H.; Drockenmuller, E.; Misner, M. J.; Russell, T. P.; Hawker, C. J. *J. Am. Chem. Soc.* **2006**, *128*, 7622–7629.
(6) Stadler, R.; Auschra, C.; Beckmann, J.; Krappe, U.; Voigt-Martin, I.; Leibler, L. *Macromolecules* **1995**, *28*, 3080–3097.
(7) Lynd, N. A.; Meuler, A. J.; Hillmyer, M. A. *Prog. Polym. Sci.* **2008**, *33*, 875–893.
(8) Sahin, O.; Magonov, S.; Su, C. M.; Quate, C. F.; Solgaard, O. *Nat. Nanotechnol.* **2007**, *2*, 507–514.
(9) Sahin, O.; Erina, N. *Nanotechnology* **2008**, *19*, 445717.
(10) Jesse, S.; Kalinin, S. V.; Proksch, R.; Baddorf, A. P.; Rodriguez, B. J. *Nanotechnology* **2007**, *18*, 435503.
(11) Stan, G.; Cook, R. F. *Nanotechnology* **2008**, *19*, 235701.
(12) Nishi, T.; Nukaga, H.; Fujinami, S.; Nakajima, K. *Chin. J. Polym. Sci.* **2007**, *25*, 35–41.
(13) Nagai, S.; Fujinami, S.; Nakajima, K.; Nishi, T. *Compos. Interfaces* **2009**, *16*, 13–25.
(14) Johnson, K. L.; Kendall, K.; Roberts, A. D. *Proc. R. Soc. London, Ser. A* **1971**, *324*, 301–313.
(15) Sun, Y.; Walker, G. C. *Langmuir* **2004**, *20*, 5837–5845.
(16) Motomatsu, M.; Mizutani, W.; Tokumoto, H. *Polymer* **1997**, *38*, 1779–1785.
(17) Wang, L.; Hong, S.; Hu, H. Q.; Zhao, J.; Han, C. C. *Langmuir* **2007**, *23*, 2304–2307.
(18) McLean, R. S.; Sauer, B. B. *Macromolecules* **1997**, *30*, 8314–8317.
(19) Han, X.; Hu, J.; Liu, H. L.; Hu, Y. *Langmuir* **2006**, *22*, 3428–3433.
(20) Ganguly, A.; Sarkar, M. D.; Bhowmick, A. K. *J. Polym. Sci., Part B: Polym. Phys.* **2007**, *45*, 52–66.
(21) Mayes, A. M.; Russell, T. P.; Deline, V. R.; Satija, S. K.; Majkrzak, C. F. *Macromolecules* **1994**, *27*, 7447–7453.
(22) Helfand, E.; Wasserman, Z. R. *Macromolecules* **1976**, *9*, 879–888.
(23) Helfand, E.; Wasserman, Z. R. *Macromolecules* **1978**, *11*, 960–966.
(24) Raghavan, D.; Gu, X.; Nguyen, T.; VanLandingham, M. R.; Karim, A. *Macromolecules* **2000**, *33*, 2573–2583.
(25) Bar, G.; Thomann, Y.; Brandsch, R.; Cantow, H. J.; Whangho, M. H. *Langmuir* **1997**, *13*, 3807–3812.
(26) Magonov, S. N.; Ellings, V.; Whangbo, M. H. *Surf. Sci.* **1997**, *375*, L385–L391.
(27) Jiao, Y. K.; Schäffer, T. E. *Langmuir* **2004**, *20*, 10038–10045.
(28) Heinz, W. F.; Hoh, J. H. *Nanotechnology* **1999**, *17*, 143.
(29) Zhou, T.; Zhang, A. M.; Zhao, C. S.; Liang, H. W.; Wu, Z. Y.; Xia, J. K. *Macromolecules* **2007**, *40*, 9009–9017.
(30) Wang, L.; Zhao, J.; Han, C. C. *Polymer* **2008**, *49*, 2153–2159.
(31) Tsukruk, V. V.; Sidorenko, A.; Gorbunov, V. V.; Chizhik, S. A. *Langmuir* **2001**, *17*, 6715–6719.